Observations of the Geminids and Quadrantids using a stratosphere–troposphere radar

P. Brown,[1,2] W. K. Hocking,[1] J. Jones[1] and J. Rendtel[2]

[1]*Department of Physics and Astronomy, University of Western Ontario, London, Ontario, N6A 3K7, Canada*
[2]*International Meteor Organization, PF 600118, D-14401 Potsdam, Germany*

ABSTRACT
Radar observations of the 1996 Geminid and 1997 Quadrantid showers are reported using the CLOVAR stratosphere–troposphere (ST) radar. A method for determining the limiting sensitivity of a radar system using observed number–amplitude data from a single shower is presented, and the result compared with more conventional measurements. This technique is capable of providing very precise measurement of the mass index for a shower in cases where large numbers of echoes are available. The mass index profiles for both showers are presented and found to be U-shaped with a minimum near the time of peak flux. Peak flux values are found to be 0.19 ± 0.02 meteoroid $\text{km}^{-2}\,\text{h}^{-1}$ at $261\overset{\circ}{.}82 \pm 0\overset{\circ}{.}2$ for the Geminids and 0.14 ± 0.01 meteoroid $\text{km}^{-2}\,\text{h}^{-1}$ at $283\overset{\circ}{.}08 \pm 0\overset{\circ}{.}08$ for the Quadrantids to a limiting radio magnitude of 7.7. The locations of maximum are found to coincide with the visually determined position. No significant difference in the location of maximum is detected for either stream over a range of 2 radio magnitudes or in comparison with the visual results. The Geminid radar flux curve is found to be very broad near maximum with a plateau in activity lasting nearly 2 d, while the visual curve shows a FWHM of 24 ± 4 h and modest asymmetry with a slow build-up to maximum. The Quadrantids are found to have a sharp maximum following a Gaussian profile to first order with a full width to the $1/e$ flux positions of 12 h.

Key words: techniques: radar astronomy – meteors, meteoroids.

1 INTRODUCTION

Radio observations of meteors using stratosphere–troposphere (ST) radars have been carried out for as long as ST radars have been in operation. Normally, meteor echoes are observed with ST radars to determine mesopheric wind patterns (cf. Hocking & Thayaparan 1997, and references therein), but some astronomically useful information is also recorded by these systems. Watanabe et al. (1992), for example, have made extensive use of the ST radar operated by Kyoto University for observations of the Perseids and the sporadic background.

A principal advantage of using an ST radar is the possibility of using information gathered for wind measurements and other projects without the need for a separate meteor radar. ST observations are often made nearly continuously and hence function as very effective meteor patrol radars. Some drawbacks may occur in this situation, however, as

meteor echo information may be deliberately filtered from the observations (such as long-enduring overdense echoes) in the process of trying to determine accurate wind information and avoid contamination from other reflections.

In this work we analyse radar observations of the 1996 Geminid and 1997 Quadrantid meteor showers using the CLOVAR (Canada London Ontario VHF Atmospheric Radar) ST radar, and compare these results with visual observations of the same showers. These observations were carried out during a campaign designed to determine the horizontal wind field over London, Ontario. We have developed novel methods for determining the limiting meteor sensitivity of an ST system and the mass index of a stream from radar observations, and present details of these techniques. The flux profiles at three different limiting sensitivities for each shower are presented and compared with visual observations, as is the mass index profile. The use of an interferometer with this system makes flux determina-

tions more accurate and also permits the generation of radiant maps.

2 EQUIPMENT AND DATA COLLECTION

The CLOVAR ST radar has been operational near London, Ontario (43°N and 81°W) since 1993 November. Extensive details of the system hardware, reduction techniques and antenna systems, as well as discussion of results and limitations related to wind measurements, can be found in Hocking (1997) and Hocking & Thayaparan (1997). Here we present basic details of the system as it relates to observations made in CLOVAR's meteor mode during 1996 December and 1997 January.

The very high-frequency (VHF) radar operates at 40.68 MHz with a peak power of 10 kW and a maximum average power of 800 W. During these observations, the radar was set to a pulse repetition frequency (PRF) of 2143 Hz and a pulse duration of 13.33 μs which translates into an actual average power output of 290 W. The system does not use pulse coding and, as such, the PRF produces an intra-pulse spacing of 70 km, which is not sufficient to avoid range aliasing of significantly off-vertical meteor echoes. When combined with the directional information from the interferometer, however, a number of possible ranges corresponding to heights within the meteor region (80–120 km) can be determined.

The transmitting antenna is a vertically directed four-element Yagi, while the receiving system is a five-antenna array of two-element vertically directed dipoles. The transmitting Yagi has a directivity of 8.7 dB$_i$, while each receiving antenna has $D = 7.3$ dB$_i$. All antennas are 0.25λ above the ground. We have found that the resulting gain patterns for both are well approximated as

$$G(\theta) = D\left[1 - \cos^2\theta \, \sin^n\left(\frac{2\pi}{\lambda} \sin \xi\right)\right], \tag{1}$$

where θ is the polar angle measured from the main axis of the array (which is aligned at 21° west of north), ξ is the angular elevation and n is an exponent associated with the ground reflection term appropriate to the antenna configuration (roughly 6 for a four-element Yagi and 2 for a two-element dipole).

The receiving array is multiplexed through a single receiver (which also includes a noise channel), and the six resulting in-phase and quadrature signals are four-point smoothed before being digitally stored on a PC. The final temporal resolution for the system is 11 ms, resulting in an effective PRF of 90 Hz. The raw digital output is searched in 30-s blocks for signals exceeding a pre-set trigger level that have characteristics consistent with meteor echoes, and the signals stored for later analysis. The detection algorithms use the signals from all five antennas after they are averaged incoherently to increase significantly the signal-to-noise ratio. Correlation techniques are then used for subsequent analysis. This procedure results in nearly a doubling of the number of detectable echoes.

The five-element receiving antenna array functions as an interferometer in a set-up designed to minimize phase errors (cf. Jones & Webster 1992). A detailed treatment relating the measured phases to equivalent direction cosines

for this system can be found in Thayaparan (1995) and references therein.

The basic spacing and layout of the receiving array are shown in Fig. 1. Ideally, any two receiving antennas can be used to provide a single direction cosine to the signal source by comparing their relative phase differences. From Fig. 1 it is readily seen that for antennas 1 and 0, spaced a distance d wavelengths apart, for example, the relative phase difference is related to the direction cosine angle via

$$\Delta\phi = \frac{2\pi}{\lambda} d \cos \theta. \tag{2}$$

As shown in the figure, the CLOVAR set-up actually uses spacings of 2λ and 2.5λ between the antennas. This implies that using the phase difference between any two antennas produces multiple possible solutions for equation (2). This spacing is optimal for an interferometer (Jones & Webster, in preparation).

Between antennas 1 and 2 (referenced to the middle antenna 0) we have

$$\phi_{10} - \phi_{20} = \pi \cos \theta, \tag{3}$$

which produces a single solution for θ. In practice, however, the phase difference may be in error by many tens of degrees as a result of noise. Since the error in the arrival direction is

$$d\theta = \frac{d\Delta\phi}{2\pi d}, \tag{4}$$

it is immediately apparent that using a larger baseline (bigger d) produces more accurate values for θ for a given phase error. Thus, once θ is determined using the difference of the difference of the phases of the outer antennas, the phase difference between antennas along longer baselines in the array can be used to refine further the initial value of θ. For

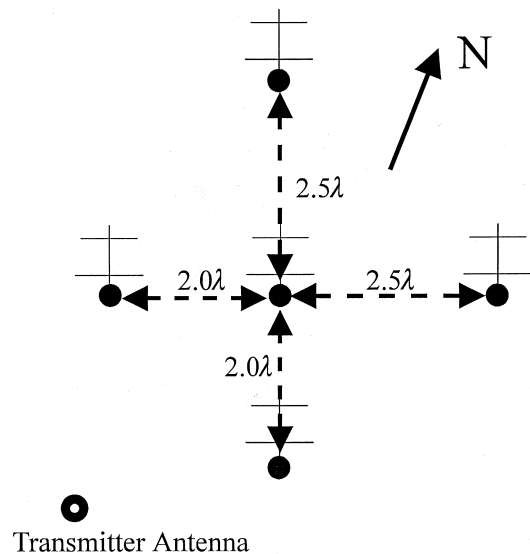CLOVAR VHF meteor radar antenna layout

Figure 1. The receiving array of an interferometer.

CLOVAR we have determined that the average angular error for a given echo is of order 2°.

3 DETERMINATION OF FLUX

To determine the relative influx of stream meteoroids to a given limiting mass from radar observations, one must know the collecting area in the atmosphere over which meteors can be detected, and also the limiting meteoroid mass observable by the radar. The collecting area for a given radiant can be found by using the fact that all short-duration echoes are specular. A recent detailed treatment and derivation of the echo collecting area has been given by Brown & Jones (1995). In general, all such treatments are derived from Kaiser (1960, and references therein), although Elford & Hawkins (1964) have independently developed an equivalent treatment for determination of the radiant response function (cf. Elford et al. 1994 for more details). In what follows, we adopt the methodology of Kaiser (1960).

3.1 Echo collecting area

For an echo from a radiant with local vector $\boldsymbol{m}$ as seen from a radar at point R to be observable, it must make a right angle with the plane of which the normal is $\boldsymbol{m}$ and the origin is R. The intersection of this plane with the meteor region in the atmosphere defines the 'echo strip' (Fig. 2). A unit area along this strip is given by

$$dA = \frac{dh\,dx}{\sin z},\tag{5}$$

where dh is the average length of the meteor trail, dx is the linear distance along the echo strip, and z is the zenith angle of the radiant. In earlier treatments (see Poole & Kaiser 1967 for a review) the height range of ablation has been derived from classical single-body meteor theory or slight modifications of it. Here we use the observational results of Flemming, Hawkes & Jones (1993) from TV observations of faint meteors to express the vertical trail lengths (in km) as an empirical function of the mass index, s, as

$$dh = 1.15 + 14.6\exp(-s/1.44).\tag{6}$$

The effective collecting area for a given radiant is found by integrating equation (5) weighted by the antenna gain along the echo strip referenced to the most sensitive direction to yield
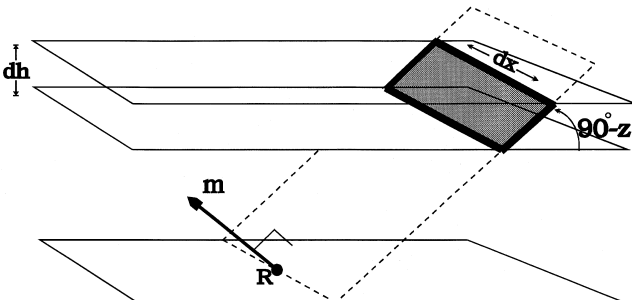

Figure 2. The echo plane and reflecting geometry.

$$A_{\text{eff}} = \int\left(\frac{G}{\cos z}\right)^{s-1}.\tag{7}$$

In practice, A_{eff} is found by integrating numerically along the echo line out to some limiting range. For CLOVAR this range is 300 km, as this ensures that echoes below 20° elevation are excluded since such echoes have the greatest angular errors. In practice, there are very few echoes at larger ranges, so this cut-off has little effect on the final numbers. Taking A_{eff} together with the observed radar shower rate, Ξ, the flux Φ can be found from

$$\Phi = \frac{\Xi}{A_{\text{eff}}}.\tag{8}$$

The determination of the flux requires a value of s. In the following section we outline a method for determining precise values of s from amplitude distributions, and also the use of this method as an independent check of the limiting sensitivity of the radar system.

3.2 Limiting sensitivity of the radar

To determine the limiting electron line density sensitivity for a radar (q_{lim}), we use the bandwidth of the receiver, B, (which is 200 kHz for the CLOVAR system) and calculate the equivalent antenna temperature from the sky noise to find the minimum detectable power as (McKinley 1961)

$$P_{\text{noise}} = 5.6 \times 10^7\, f^{-2.3}\, k_{\text{B}} B,\tag{9}$$

where f is the frequency and k_{B} is Boltzmann's constant. At VHF frequencies the cosmic noise completely dominates receiver noise; we include no additional correction for the small contribution to the total equivalent temperature from the receiver. Using 200 kHz for B produces a value of $P_{\text{noise}} = 3 \times 10^{-14}$ W, the theoretical limit for detectability to the cosmic noise floor. In practice, only those echoes approximately 10 dB above this limit will actually be detected, so the effective detection threshold is $P_{\text{th}} \approx 3 \times 10^{-13}$ W. For a transmitted power of P_{th} and a directivity D at range R, this minimum threshold power corresponds to a minimum detectable line density of (McKinley 1961)

$$q_{\text{lim}} = \sqrt{\frac{P_{\text{th}} R^3}{2.5 \times 10^{-32} P_{\text{t}} D^2 \lambda^3}},\tag{10}$$

where all units are MKS (metres, kilograms seconds). For CLOVAR with the minimum range of 100 km and P_{th} of 3×10^{-13} W, this yields $q_{\text{lim}} = 8.7 \times 10^{12}$ electron m^{-1}. Use of the relation between magnitude and line density of

$$M_R = 40 - 2.5\log_{10} q\tag{11}$$

shows that this q_{lim} corresponds to a meteor of magnitude $+7.7$. This is the theoretical estimate for the limiting meteor sensitivity for CLOVAR. An alternative method uses the distribution of echo amplitudes and the 'knee' in the number–amplitude distribution as a fiducial point for determination of the same value. A rough outline of the principles of this method was first presented by Kaiser (1955). We next describe this technique in detail.

3.3 Method for finding the mass index (*s*)

The distribution of meteor echoes as a function of electron line density is assumed usually to follow a power-law relation of the form

$$N(q) = \frac{K}{s-1} \, q^{1-s}, \tag{12}$$

where $N(q)$ is the cumulative number of echoes with line densities of q or more, K is a constant and s is the differential mass index. Note that it is implicitly assumed that a similar relation (with the same exponent s) exists for the mass distribution which is equivalent to assuming that $q \propto m$.

The amplitude received owing to specular scattering from a meteor trail depends on the electron line density. The functional dependence on q is determined by the regime of scattering – either underdense or overdense. Underdense echoes produce $P_r \propto q^2$ whilst overdense echoes have $P_r \propto q^{1/2}$, where P_r is the received power. This change in the scattering properties implies that the number distribution of echo amplitudes ($\sqrt{P_r}$) will follow $N(q) \propto q$ for underdense echoes and $N(q) \propto q^{1/4}$ for overdense echoes. Thus, in the region near the transition line density ($q \approx 2 \times 10^{14}$ m^{-1}), a steep downward shift in the slope of the number–amplitude distribution occurs. This change in scattering properties, as well as the change in the limiting sensitivity with range (i.e. for larger echo ranges the transition knee is preferentially shifted to smaller echo amplitudes), leads to the final shape of the number–amplitude distribution (cf. Šimek 1987). Fig. 3 shows the number–amplitude distribution for Quadrantid meteors on 1997 January 3. The change in slope and 'knee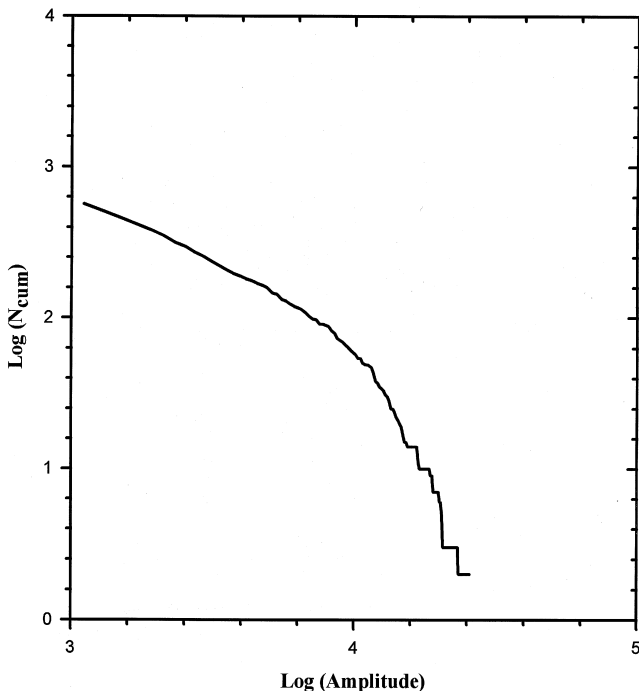' near amplitude values of $\approx 10\,000$ is clear. A comparison of the theoretical position of the knee with its observed location allows for the use of this knee feature as an absolute calibration for the system.

To produce a theoretical version of this curve, we use equation (5), equation (12) and the number amplitude dependence of the scattering on q, and make two discrete sums in the numerical integration for each echo line depending on whether the line density sensitivity at a given point is above or below the transition line density. By varying the assumed limiting line density it is possible to construct the relative theoretical number of echoes of amplitude A or larger expected for any value of q_{lim}. Thus we have

$$T_{\mathrm{num}} = \left[\sum_{\mathrm{under}} \left(\frac{q}{q_{\mathrm{ref}}} \right)^{1-s} + \left(\frac{q_{\mathrm{trans}}}{q_{\mathrm{ref}}} \right)^{1-s} \sum_{\mathrm{over}} \left(\frac{q}{q_{\mathrm{trans}}} \right)^{4(1-s)} \right]$$
$$\times \, \mathrm{d}h(s) \, \tan \xi \, \mathrm{d}x, \tag{13}$$

where q is the local limiting line density at any given point on the echo line, q_{ref} is an arbitrary reference line density, $q_{\mathrm{trans}} = 2 \times 10^{14}$ m^{-1}, and the summations are performed over each discrete step in linear distance ($\mathrm{d}x$) along the echo line. Each value for T_{num} is calculated in small steps of q_{lim}, and for each value of q_{lim} a daily 'average' is taken by evaluating (13) for a given radiant (corresponding to a single fixed echo line) at intervals of 30 min throughout the day. Since echoes beyond 300 km are not counted by CLOVAR owing to their low elevation (and hence large phase error), the summation cuts off at this distance. This also implies that no echoes from a particular radiant are detectable by the system [or counted in the summations in (13)] if the shower radiant exceeds 70° elevation. Fig. 4 shows the result
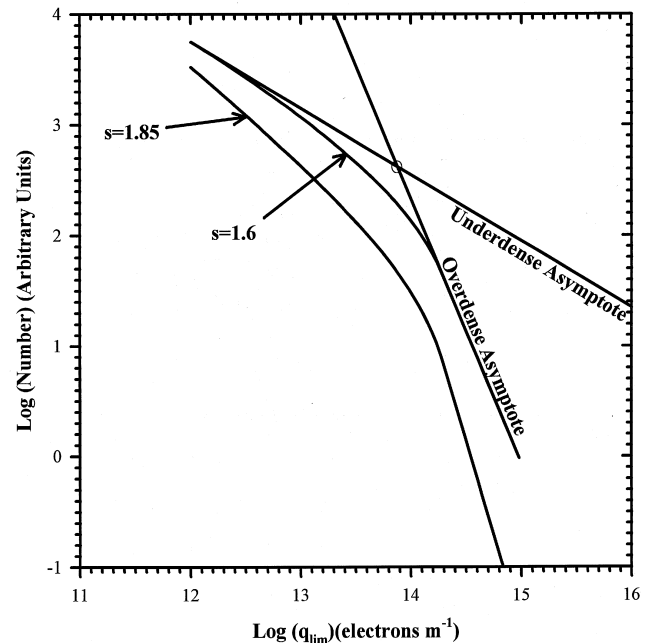

Figure 3. The cumulative distribution of echoes from the Quadrantid shower observed on 1997 January 3.

Figure 4. The theoretical shape of the number–amplitude relation for the Quadrantids for $s = 1.6$ and 1.85. The asymptotes in the underdense and overdense limits are shown for $s = 1.6$, and their cross-over position (fiducial point) is shown with an open circle.

for the Quadrantids for two values of *s*. Note the similarity to Fig. 3.

For a comparison of these curves it is necessary to relate the observed echo amplitudes to the line density. By taking the asymptotes in the extreme overdense and underdense regimes (as shown in Fig. 4), we establish a cross-over point which can be used in principle as a fiducial marker to relate the two curves. The only uncertainty is the unknown value for *s* for any particular day and shower. However, when the intersection point of the asymptotes is computed for many values of *s* for both the Geminid radiant and the Quadrantid radiant, it is apparent that this value is very robust and changes negligibly over a wide range of *s*. The variation in the asymptote intersection for various values of *s* is shown in Table 1.

As most showers have values for *s* between 1.5 and 2.0, this method offers the possibility of providing an accurate, independent calibration of the system sensitivity. This technique assumes that all echoes visible over the echo line are recorded (both overdense and underdense) to the limiting sensitivity of the system, and also that the specular condition holds for all echoes. The latter condition will eventually break down in the extreme overdense limit, but generally not until echo durations of many seconds are reached [cf. McIntosh (1966), who suggested that scattering becomes omnidirectional when durations of 10 s are reached for an all-sky system at 30 MHz]. The data collection algorithms employed by CLOVAR produce an additional complication: all echoes that do not show amplitude attenuations of at least a factor of 2 compared with the initial peak within 0.7 s are rejected. This helps to eliminate erroneous signals from aircraft, but also strongly biases against very long over-dense echoes. However, while the number of rejected echoes will be quite small (for CLOVAR an overdense echo lasting 0.7 s corresponds to $q \approx 2 \times 10^{15}$ m^{-1}) and so will not significantly affect flux values, they will have a noticeable effect on the number–amplitude curve at the top end. Indeed, it is apparent for this reason that the slope in Fig. 3 is much steeper than in Fig. 4 for the oversense asymptote. We have made an approximate empirical estimate of this effect and find that the resulting cross-over point falls within the range $3.9 < \log_{10} A < 4.0$, where A is a digital representation of the total signal voltage. Note that saturation of the

system occurs near $A \approx 30\,000$. The effective limiting amplitude sensitivity for the system (equivalent to 10 dB above the cosmic noise floor) is $A = 10^3$. This implies a shift of 0.9–1.0 in log A between the cross-over fiducial point and the limiting sensitivity value. Using the values from Table 1, and taking $q \approx 6.5 \times 10^{13}$ m^{-1} as a representative value for $1.5 < s < 2.0$, yields an equivalent limiting sensitivity of $q = 7.4 \pm 0.9 \times 10^{12}$ m^{-1}. This result compares favourably to the previously determined value from system-only considerations of 8.7×10^{12} m^{-1}. A similar analysis for the Geminids yields values closely distributed about this point and indistinguishable from the system-determined value within the errors.

The above analysis confirms our earlier results concerning the limiting sensitivity of the system, and immediately leads to an accurate method for determining values for *s*. Previous attempts to find *s* from radar data either have used overdense durations (cf. Kaiser & Closs 1952), which are necessarily limited to meteors with $q > 2 \times 10^{14}$ m^{-1} and assume diffusion-limited durations, or have assumed a linear fit for the underdense number–amplitude relation (cf. Browne et al. 1956). Inspection of Fig. 4 shows that the theoretical number curve assumes its asymptotic value only near $q \approx 10^{12}$ m^{-1}. For values of q higher than this, a significant downward curvature in the number distribution implies that all such earlier measurements are overestimating systematically the true value for *s*. This deviation from the true value for *s* will be particularly large as the transition line density is approached.

To compute a value for the mass index from CLOVAR number–amplitude distributions, we make use of the fact that the most accurate portion of the curves is from the limiting sensitivity (which is itself 10 dB above the noise floor) to a slightly higher limiting value where the effects of the 0.7 s duration echo filtering are not significant. The interval relatively unaffected by the filtering, which also has large numbers of echoes, is found to be $8.7 \times 10^{12} < q < 3.2 \times 10^{13}$ m^{-1}. We use this interval in what follows.

For each value of *s* from 1.1 to 4.0 for both the Quadrantids and the Geminids, a table of equivalent theoretical values is computed from equation (13). The values were computed at intervals corresponding to the bin sizes for the amplitude distributions (200). The best-fitting *s*-value is then found by comparing the two curves after normalizing the observed cumulative amplitude numbers and taking the sum of the square of the difference between the observed and theoretical numbers via

$$\sigma^2 = \sum_{i=1}^{17} \left(\frac{O_i T_1 / O_1 - T_i}{T_1} \right)^2 \tag{14}$$

where T is the log of the theoretical number in bin *i* for the given value of *s*, O is the log of the observed number, and the summation is over the 17 bins within our chosen interval. The value of *s* producing a minimum in σ^2 is then taken as the most probable value.

Errors in *s* are found through simulation whereby the observed number of echoes in each bin is replaced with a number chosen at random from Poisson distributions from the observed number. These new differential distributions are then summed to form a new cumulative distribution. An

Table 1. Asymptotic cross-over for the theoretical number–amplitude curve as a function of the mass index, *s*, for CLOVAR. Values given are for the Quadrantid radiant; very similar values are found for the Geminid radiant.

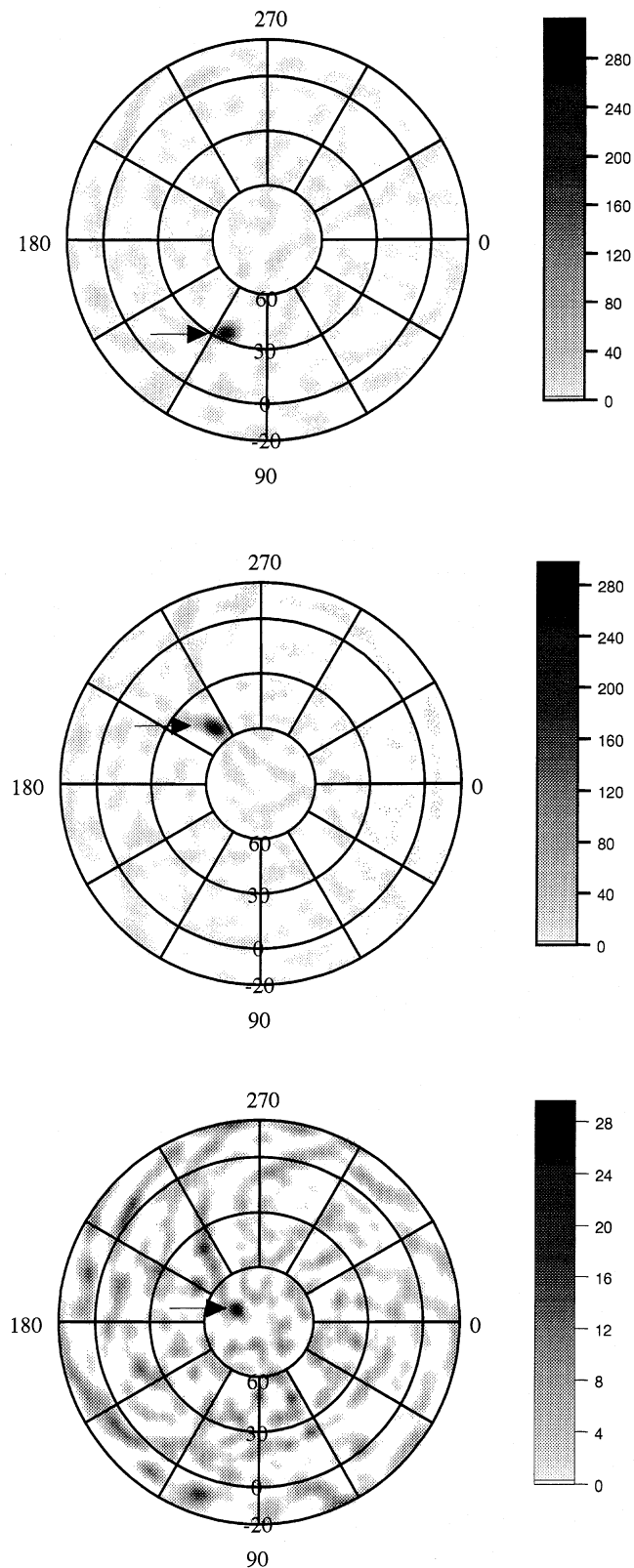| *s*	Cross-over *q*
1.5	6.3×10^{13}
1.6	6.6×10^{13}
1.7	6.8×10^{13}
1.8	6.7×10^{13}
1.9	6.5×10^{13}
2.0	6.3×10^{13}
2.1	4.8×10^{13}
2.2	3.6×10^{13}
2.3	2.9×10^{13}

Figure 5. Radiant maps for (top) the Geminid shower on 1996 December 13, (middle) the Quadrantids on 1997 January 3, and (bottom) 1996 December 22. The azimuthal angle in these plots is right ascension (α) and the polar angle is declination (δ). All values are referenced to equinox 2000. Note the presence of the radiant from the weak Ursid shower in the bottom panel at $\alpha = 217°$ and $\delta = +79°$.

appropriate s-value for each of these new distributions is then found using (14). A total of 10 000 such randomly generated distributions are made for every measured value of s, and the resulting standard deviation of the distribution used as the error.

4 OBSERVATIONS

The CLOVAR system was run continuously from 1996 December 10 until 1997 January 14, covering the activity periods of the Geminids and Quadrantids. From observations in past years it may be concluded that these are the two strongest showers visible to the radar. The typical number of echoes recorded on an average day by CLOVAR is roughly 800, but this rises by as much as 50 per cent or more during the peaks of these showers.

To determine which echoes belong to the showers, we used directional information provided by the interferometer in conjunction with the known position of the radiants. If the echoes occurred within a strip orthogonal to the radiant and 5° wide they were accepted as shower members. Note that the sporadic contamination is minimized in this way, and for most of the period is much less than 10 per cent of the total number of shower echoes. This method also permits very low shower activity to be distinguished from the sporadic noise.

These same data were used in conjunction with the radiant mapping technique of Jones (1977). For the present analysis, the weighting function for each echo was chosen according to the variation of this radiant mapping method of Jones & Jones (in preparation). The final result of this radiant mapping is found in Fig. 5 which shows the radiant maps for the peaks of the Geminids and Quadrantids, and an intermediate day with no shower activity. The apparent rms width and position of the Geminid radiant on a daily basis are given in Table 2.

The Geminid flux in 2-h bins calculated according to the method in Section 3 is shown in Fig. 6 to three limiting electron line densities for the entire period of its visibility. We refer to these limiting values as level I, II and II class echoes respectively. The variation in the mass index for the stream is given in Fig. 7. Similar plots for the Quadrantids are shown in Figs 8 and 9.

To complement these radar observations (which are nearly continuous owing to the northerly declination of the radiants), we used global visual observations of the 1996 Geminids and 1997 Quadrantids from data stored by the International Meteor Organization (IMO), shown in Figs 10–13. These visual observations were gathered and

Table 2. Radiant position and diffuseness as a function of date in December during the 1996 Geminids. The right ascension (α) and declination (δ) of the radiant are given in J2000.0 and the size of the radiant is the measured rms width in degrees.

Day	α	δ	Apparent width
10	109°.5	33°.2	5°.4
11	111°.2	35°.7	6°.1
12	112°.2	34°.5	4°.8
13	113°.9	34°.5	5°.0
14	114°.7	35°.0	12°.6
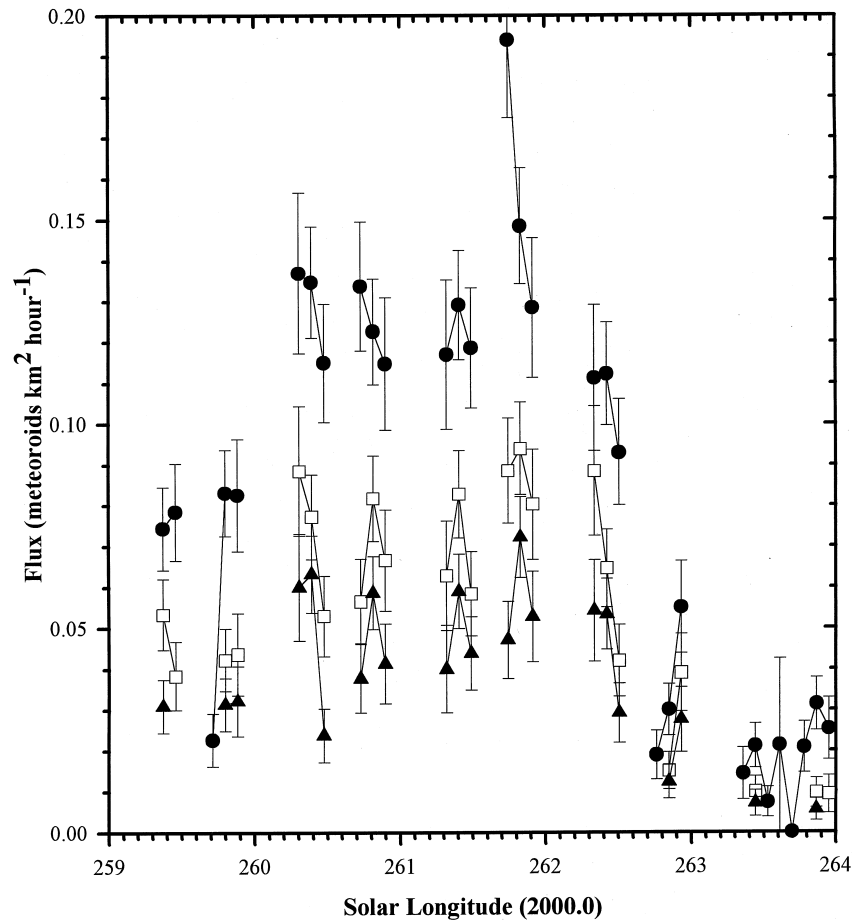
Figure 6. Flux for the Geminids for limiting values of q of 8.7×10^{12} (filled circles), 1.6×10^{13} (open squares) and 2.5×10^{13} (filled triangles) m^{-1}. These q-values correspond to Geminids of magnitudes $+7.7$, 7.0 and 6.5 respectively, and these represent level I, II and III categories of echoes hereafter.
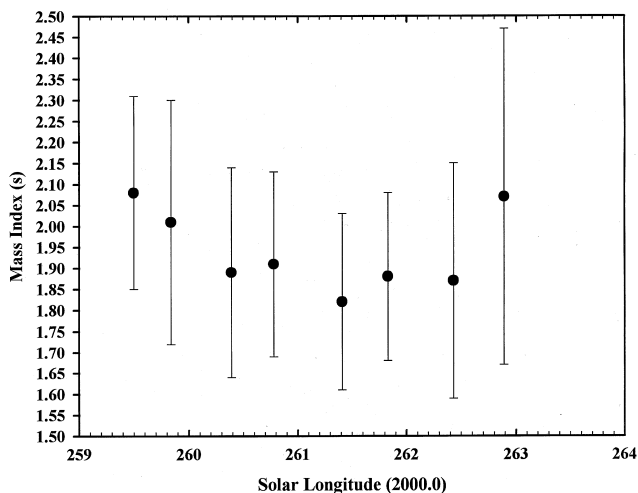

Figure 7. Variation in the mass index for the Geminids from radar observations.

analysed using the method described in Brown & Rendtel (1996).

In total 20 392 Geminids were recorded for these profiles by nearly 200 global observers in 1996. For the Quadrantid visual observations a total of 700 shower members were recorded by 30 observers. The time coverage and numbers for the Quadrantids in 1997 are very poor, and the resulting flux profile uncertain.

5 RESULTS AND DISCUSSION

5.1 Geminids

The Geminid stream is the highest flux visual shower currently visible from Earth (Rendtel et al. 1995). The maximum which occurs near December 13 each year is relatively broad, with significant activity persisting for a full day about maximum, and with some activity from the shower discernible for as much as 10 days. The shower is unusual in several respects: it has a very short-period orbit compared with other showers, and it is associated with the asteroid 3200 Phaethon. Some evidence suggests that Phaethon may be an extinct cometary nucleus (Gustafson 1989), although direct observations of the asteroid (cf. Luu 1993) suggest that it may be more asteroidal than cometary.

Over the last 40 yr, observational information concerning the flux of the shower has been limited largely to radar observations, although several recent analyses of visual observations of the stream have been made (cf. Arlt & Rendtel 1994). The most widely cited properties of the
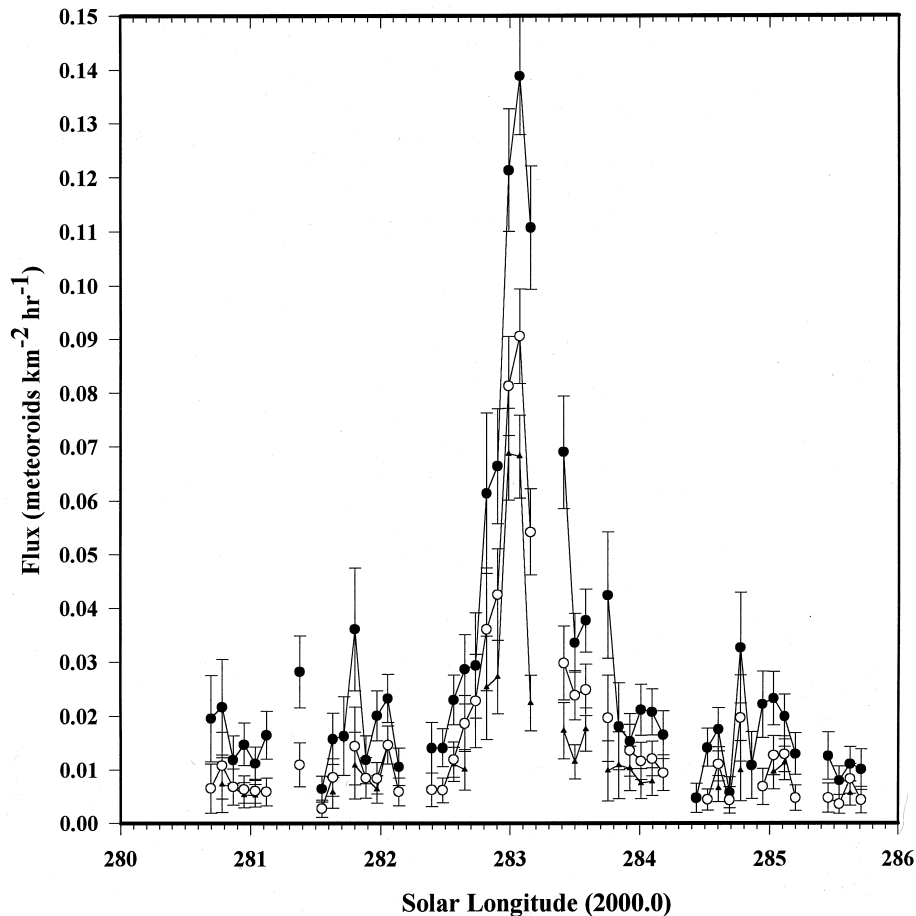
Figure 8. Flux for the Quadrantids for limiting values of q of 8.7×10^{12} (filled circles), 1.6×10^{13} (open circles) and 2.5×10^{13} m^{-1} (small filled triangles). These q-values correspond to Quadrantids of magnitudes $+7.7$, 7.0 and 6.5 respectively.
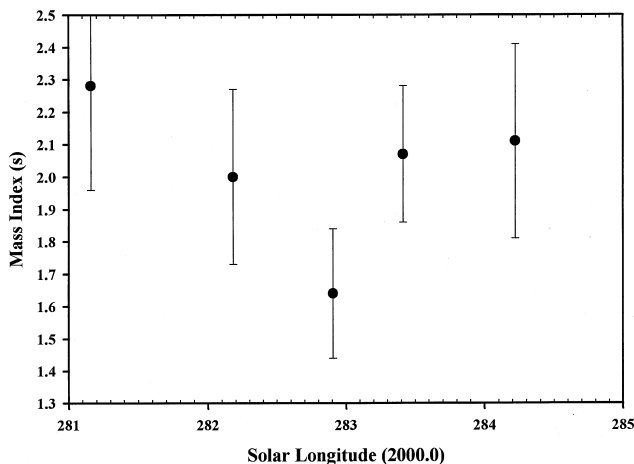

Figure 9. Variation in the mass index for the Quadrantids from radar observations.

stream from radar observations include an asymmetry in the flux profile with a gradual build-up to maximum being followed by a quick decline to background levels, typically within a day after the maximum (Hajduk, McIntosh & Šimek 1974; Jones & Morton 1982; Šimek 1985), and size sorting within the stream, wherein smaller stream meteo-

roids are encountered first, followed by larger particles later in the shower (Plavcova 1962; McIntosh & Šimek 1980). This latter observation has been interpreted as an effect arising from Poynting–Robertson drag shrinking and circularizing the orbits of smaller Geminids, and therefore placing them preferentially on the inner portion of the stream which the Earth encounters first during the shower period each year (cf. Jones 1978).

The asymmetry in the shape of the flux curve is evident in the visual flux profile of the stream in 1996 from Figs 10 and 11. This flux profile is $1°.0 \pm 0°.2$ wide to the half-maximum points with a maximum at $261°.82 \pm 0°.2$. The radar profile shows this property to a much greater degree for level I class echoes. The profile is extremely broad and shows an even more pronounced asymmetry, with a very ill-defined maximum near $261°.75 \pm 0°.1$. To a limiting magnitude of $+6.5$ (level III) – which is nominally equivalent to the visual limiting magnitude – the radar curve is much broader than the visual flux profile, but does show a modest increase to a maximum near $282°.0$ in general agreement with the visual observations. The large discrepancy in the shapes of the profiles prior to maximum is due in part to the noisiness of the radar data resulting from low numbers of echoes in some 2-h bins, and also to the uncertainty in the validity of equation (11) in relating q to M_V, as this relation was derived for brighter visual meteors.
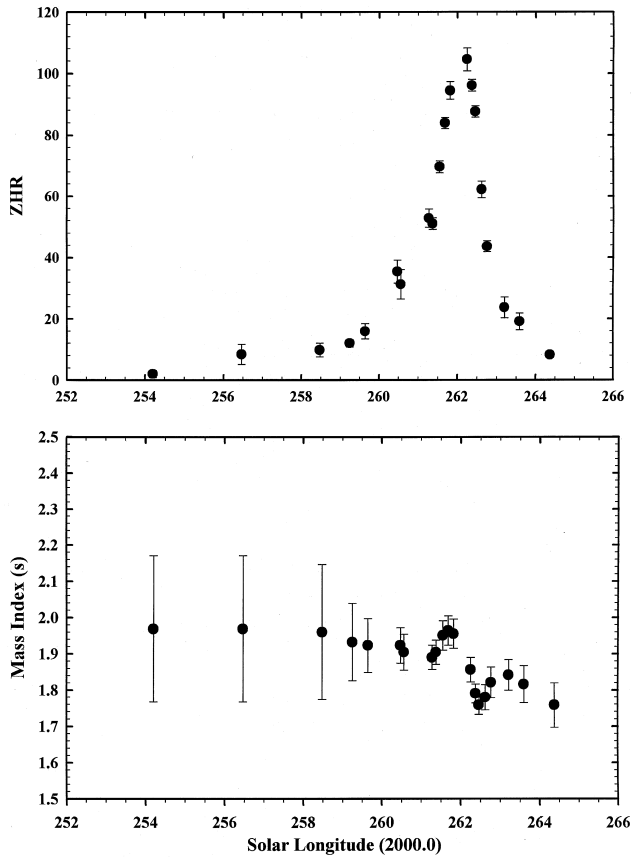
Figure 10. Visual observations of the 1996 Geminids showing the zenith hourly rate (ZHR) and mass index as a function of solar longitude (J2000.0).
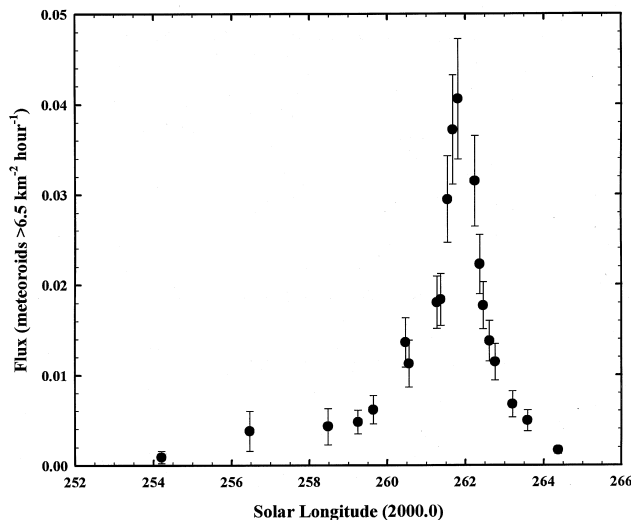

Figure 11. Flux of the 1996 visual Geminids to a limiting visual magnitude of +6.5.
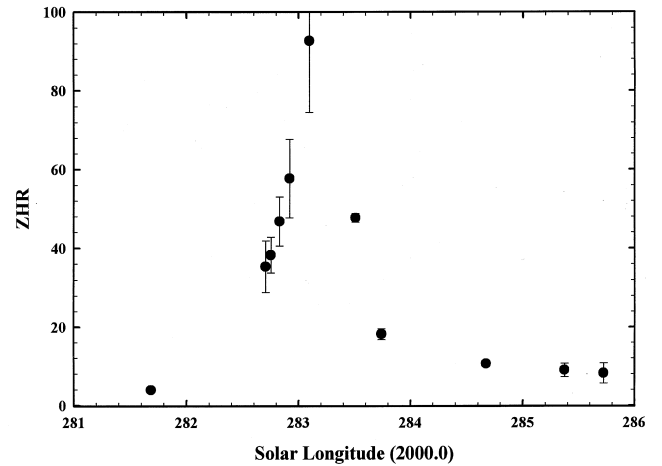

Figure 12. Visual observations of the 1997 Quadrantids showing the ZHR as a function of solar longitude (J2000.0). As discussed in the text, too few observations were available to produce a reliable value for the mass index profile, and thus a value of $s=1.80$ was used for the visual observations.
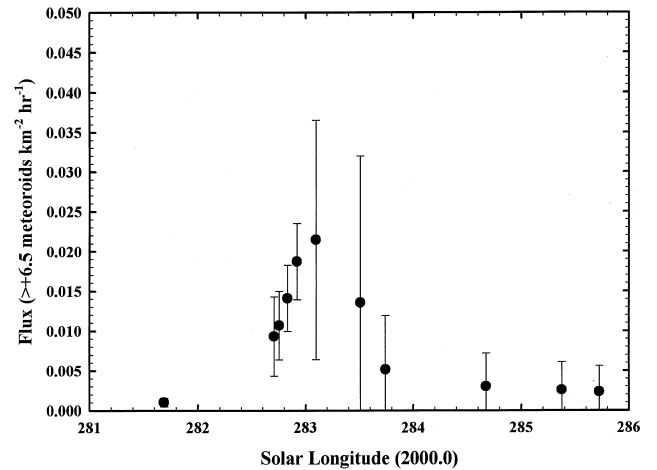

Figure 13. Flux of the 1996 visual Quadrantids to a limiting visual magnitude of +6.5.

The mass indices derived visually and by radar agree. The large errors in the radar mass index measurements can be directly attributed to the relatively small number of echoes (fewer than 500 for any one case) in the cumulative plots used to construct the s-profile. Nevertheless, the curves are in qualitative agreement, with the minimum in the radar s-profile occurring near maximum activity, as also seen in the visual results. It should be noted that the visual profile for s is extremely precise, owing to the large data set – the marked local maximum near 261°.7 followed by a local minimum near 262°.5 is probably attributable to the size sorting mechanism previously noted. This suggests that over the magnitude regime approximately 4–5 mag brighter than the limiting visual magnitude (where the vast majority of the visually recorded meteors are found), most of the difference in time of peak activity occurs within less than a 24-h period. This is in excellent agreement with the variation in time of peak as a function of magnitude constructed by Jones (1978), which suggests that in the interval $6.5 < M_V < 1.5$ the time of peak should differ by 0°.8. Note that the radar sampling interval is too large to show such fine detail.

The absolute levels of the peak fluxes to the same limiting magnitude (0.04 meteoroids km^{-2} h^{-1} for visual and ≈ 0.07

meteoroid km^{-2} h^{-1} to level III for radar) are in agreement within the uncertainties of observation. Here the uncertain magnitude scale is compounded by an additional uncertainty in the absolute value of the collecting area resulting entirely from the large errors in *s*. To demonstrate how sensitive the absolute flux levels are to *s*, we show the variation in integrated daily collecting area from the Geminid radiant for CLOVAR as a function of the mass index in Fig. 14. For all flux calculations for the Geminids, a mean *s*-value of 1.90 (which is most representative of the entire period of activity) was chosen. It is clear from Fig. 7 that the true value of *s* in many intervals might be as low as 1.6, reducing the flux by a factor of more than 2, and accounting entirely for the difference in absolute fluxes.

Comparison of our results with earlier work is not straightforward, in view of the variations in activity and position of maximum for the Geminids, an effect noted by McIntosh & Šimek (1980) from long-term radar observations of the shower. They showed that maximum activity at any given magnitude level can vary by as much as a degree in solar longitude and by more than a factor of 3 in peak flux. The latter result may be due to the short period of the stream, and also to the possible youth of the shower; such factors would naturally lead to large interannual variations.

The diffuseness of the radiant as a function of solar longitude (Table 2) shows no clear pattern except a contracton near the time of maximum. This is in contrast to the general decrease in radiant width as the shower progresses, noted by Jones & Morton (1982). We believe that our radiant widths are limited by the large angular errors for individual echoes and do not reflect any true physical variations. This conclusion is further reflected by the fact that the radiant size is found to be anticorrelated with the number of Geminids in the sample.

5.2   Quadrantids

The Quadrantid stream peaks each year near January 3 and is among the strongest of the annual showers. Like the Geminids, the Quadrantids are known to show considerable
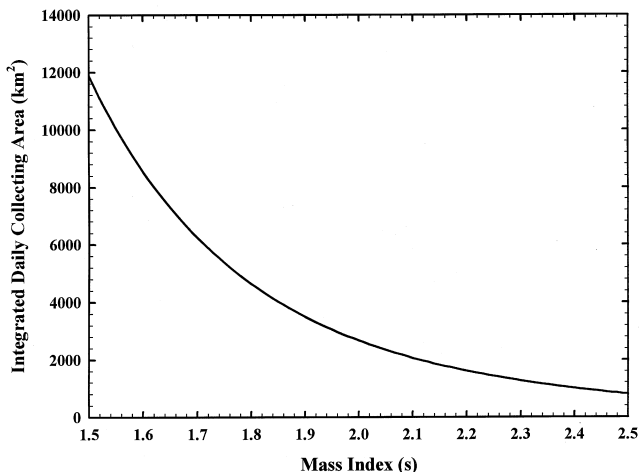

Figure 14. Integrated daily collecting area for CLOVAR for the Geminid shower as a function of the mass index (*s*).

variations in peak flux and position of maximum from year to year. These effects result from the close approach of the stream to Jupiter (Murray, Hughes & Williams 1980), and to some stream members having semimajor axes placing them close to the 2:1 resonance with that planet (Froeschle & Scholl 1982). Impulse effects arising from Jovian perturbations have been definitively observed in connection with the 1987 return of the shower (Ohtsuka, Tashikawa & Watanabe 1995), confirming the close coupling of the stream to Jupiter. The parent of the Quadrantids is still not known for certain, but both 96P/1986 J2 (Machholz 1) (Jones & Jones 1993) and Comet C/1490 Y1 (Williams & Wu 1993) are possible candidates.

Like the Geminids, the Quadrantids have been observed to show a mass-dependent time of maximum, with larger meteoroids peaking later (Hughes & Taylor 1977). Unlike the Geminids, however, the high inclination of the Quadrantids excludes this factor being due to the Poynting–Robertson effect; rather, there has been the suggestion that it is related to the variation in aphelion distance as a function of mass affecting encounter conditions with Jupiter and thus nodal regression rates (Hughes, Williams & Fox 1981).

The radar flux profile from 1997 shows a very strong, concentrated maximum at $283°.08 \pm 0°.08$ over all three radar thresholds. For comparison, the visual flux profile, which is less precise for the Quadrantids than for the Geminids, shows a maximum at $283°.1 \pm 0°.1$, in good coincidence with the radar time of maximum. Hughes & Taylor (1977) derived a relation between the time of maximum and the magnitude (*M*) from radar observations of

$$\lambda_\odot = 283.95 \pm 0.04 - (0.109 \pm 0.01)\,M, \tag{15}$$

valid in the interval $2.3 < M < 7.2$, which would suggest that, for the magnitude difference between level I and level III radar meteors, a difference of $0°.13$ in maximum should be observed, with the brighter meteors peaking later. This effect is not observed, and inspection of Fig. 8 shows some indication that just the opposite trend is occurring, although this is not significant within the stated error margins. That this is not an implausible result follows from a similar relation determined for the stream from radar observations by Šimek & McIntosh (1991), where only a small shift in time of maximum with meteor magnitude class was noted, the shift in fact being zero within the errors. It is important to note, however, that the latter result applies principally to brighter meteors ($M_V = +3$).

The flux profiles are quite symmetric, and following Rendtel et al. (1996) we have attempted a non-linear regression fit of the radar flux profiles with a Gaussian of the form

$$\Phi = \Phi_0 \left\{ \frac{1}{\sigma\sqrt{2\pi}} \exp\left[-\frac{1}{2}\left(\frac{\lambda_\odot - \lambda_{\odot\,\mathrm{max}}}{\sigma} \right)^2 \right] \right\}, \tag{16}$$

where σ is the Gaussian width of the profile and Φ_0 is a measure of $\sigma\sqrt{2}\pi\Phi_{\mathrm{max}}$, Φ_{max} being the peak flux at the position of maximum, $\lambda_{\odot\mathrm{max}}$. A fit to the flux profile for level I class echoes is shown in Fig. 15. That the central portion of the Quadrantid flux profile is Gaussian to first order has been previously noted by Hughes & Taylor (1977), and used by McIntosh & Šimek (1984) to fit long-term rate profiles of
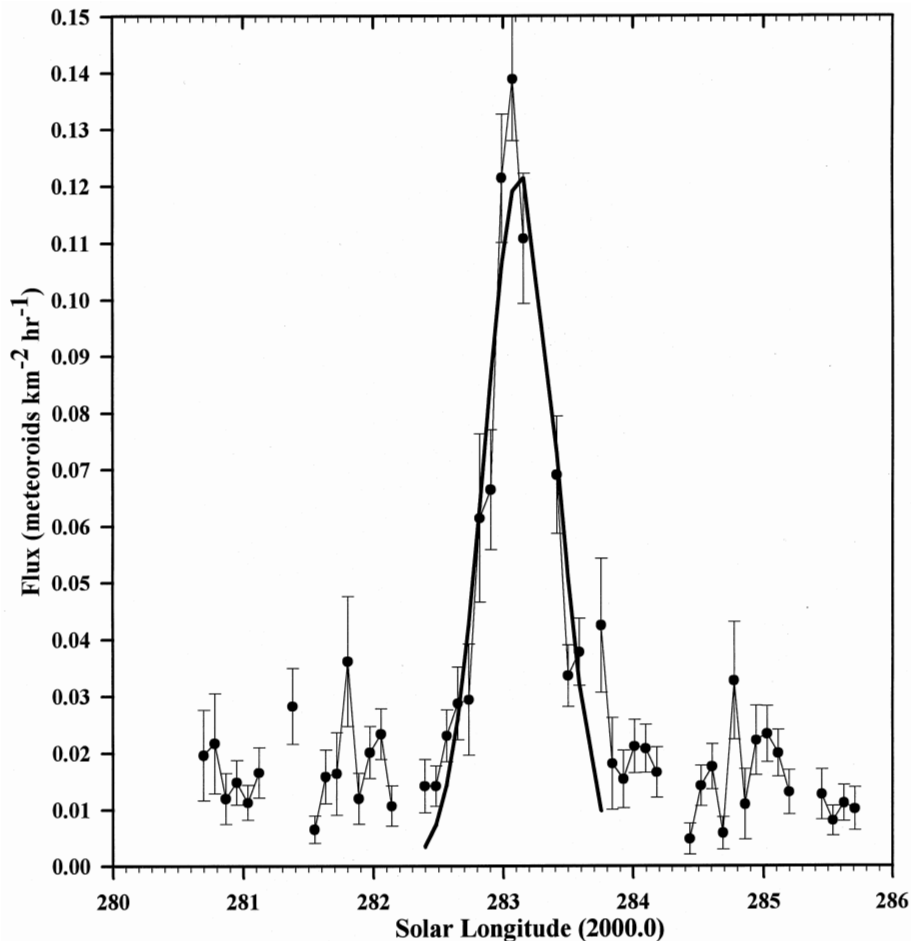
Figure 15. Gaussian fit to the radar flux profile for level I class Quadrantid echoes.

the stream. It was noted by Šimek & McIntosh (1991) that these same data showed only a rough fit to a Gaussian profile, being higher at maximum than predicted solely on the basis of a Gaussian fit. We observe the same effect, and suggest that this may lend support to the notion that an innercore of higher activity exists within the stream, as first noted by Bullough (1954). Table 3 summarizes the widths and positions of maximum determined with the Gaussian fit for each flux profile from levels I–III.

A trend toward smaller widths at larger masses is evident and expected on the basis of the initial ejection conditions and orbital evolution of the particles, but is not significant within our errors. Similarly, the trend to earlier positions of maximum for larger particles is opposite to the commonly espoused trend, but also may not be significant within our errors. Šimek & McIntosh (1991) have shown that the position of maximum activity varies by as much as $0°15$ from year to year, owing presumably to the influence of Jupiter. They have also shown that in any one year the fluctuations in the time of maximum resulting from this effect may overwhelm the mass sorting trend, and have also noted reversed trend years similar to what is hinted at in our radar observations.

The variation in the mass index across the stream also shows large error margins for the same reasons as discussed

Table 3. Gaussian widths (σ) and positions of maximum ($\lambda_{\odot\,\mathrm{max}}$) for each echo class (I–III), corresponding to radio magnitudes of 7.7, 7.0 and 6.5 respectively for the 1997 Quadrantids.

Level	σ	$\lambda_{\odot\,\mathrm{max}}$
I	$0°28 \pm 0°02$	$283°14 \pm 0°03$
II	$0°27 \pm 0°03$	$283°10 \pm 0°03$
III	$0°23 \pm 0°05$	$283°06 \pm 0°06$

in connection with the Geminids. The qualitative shape of the curve suggests a broad minimum near the time of flux maximum, in general agreement with the radar observations of Poole, Hughes & Kaiser (1972) and Bel'kovich, Sulejmanov & Tokhtas'ev (1984); both groups of authors observed a deep minimum to a value near $s=1.7$ at $283°2$ and $283°4$ respectively. Both groups of authors also report the values returning to near $s=2$ within $1°$ on either side of this position.

The absolute levels of peak flux of the visual and radio (level III) echoes show an almost identical discrepancy to that for the Geminid flux curves in terms of both direction and magnitude, the visual flux being a factor of several too low. Here again, the same explanation holds, namely that

the mean *s*-value used for computing the collecting area ($s = 1.75$) is almost certainly significantly different across the stream, given the large error values, and a similar uncertainty exists in converting magnitude to electron line density.

6   CONCLUSIONS

We have described the usefulness of the CLOVAR ST radar in collecting astronomically interesting meteor information at the same time as the system is involved in performing wind measurements, using the 1996 Geminid and 1997 Quadrantid showers as examples. The use of an interferometer with this system makes shower identification and flux profiles more accurate than with statistical methods to remove the sporadic background used for other meteor radars.

In using the known system properties and applying the collecting area theory of Kaiser (1960), we have shown how absolute levels of flux may be derived from such a system. We have also developed in detail a method involving the number–amplitude distribution observed by CLOVAR for a particular shower, which permits a check on the system sensitivity. It is found to provide good agreement with the classically determined value from system parameters, and we find that CLOVAR's limiting meteor sensitivity is $q = 8.7 \times 10^{12}$ m^{-1} within the errors for both measurement techniques.

Using the same theoretical approach to the number–amplitude distribution, we have also been able to determine the mass index for each shower as a function of time. The precision of individual measurements is low in the present case, owing to the relatively small number of echoes collected from the shower each day, but the method offers the promise of very precise measures of mass indices for systems with large shower data rates. Past use of the number–amplitude method in radar work for determining *s* may systematically overestimate this value, particularly for systems that have limiting electron line densities well above $\approx 10^{12}$ m^{-1}.

The position of the peak for the 1996 Geminid shower is found to be the same for level I, II and III class echoes, and also for the visually determined flux peak. The best estimate for the peak of the shower in 1996 within the magnitude range $7.7 < M < 6.5$ as determined by both radar and visual observations is $261°\!.8$ with an uncertainty of approximately 2 h. Through comparison of the radar and visual profiles, there is evidence that the shower profile is asymmetric and that this is more pronounced for the fainter (radar) meteors. The width of the stream profile to the half-maximum points from the visual data is $0°\!.5$ within the errors, implying that the central visual portion of the stream is active for about 24 h. The asymmetric profile is most obvious at the quarter-maximum points where the width is 10 after maximum. For level I class echoes, the values for half-maximum points are approximately $2°$ before maximum and $1°$ after maximum, while the widths to the quarter-maximum points are $> 3°$ pre-maximum and $1°\!.3$ post-maximum.

The Quadrantid radar flux profile is much narrower and smoother than the Geminid curve. The radar flux profiles are, to first order, Gaussian in shape and show a tendency toward smaller widths at larger masses. The full Gaussian width of the Quadrantid flux profile (e.g. to 1/e maximum activity) is order of 12 h. Our value is significantly less than the half-strength profile widths measured by Šimek & McIntosh (1991) from smoothed profiles covering several decades of observation. In particular, for their faintest magnitude class ($+6.0$) they measured a full width to half-maximum of $1°\!.3$. The factor of nearly 3 difference in the two measures is almost certainly due to the smearing effect of combining many sets of observations, particularly when the peak position moves from year to year, an effect discussed extensively by Šimek & McIntosh (1991).

Within the limits of our observational error, none of the measured radar echo classees differed as to their time of peak flux, nor did these data vary from the visually determined time of peak in 1997.

The peak flux values for level III class Geminid and Quadrantid echoes and the visual flux do not agree within the 67 per cent formal error limits. The lower value of the visual flux (a factor of ≈ 2–3 below the radar values) is partially the result of the uncertain magnitude–electron line density relationship. Also, in calculating the fluxes we have made the simplifying assumption that *s* remains constant. In fact, the mass index probably depends on position within the stream, and this breakdown of our constant-*s* assumption also contributed to our quoted flux variances. That the visual flux is below the radar flux value suggests either that the effects of initial train radius attenuation are not severe for these two showers, or that our collecting areas are greatly underestimated.

REFERENCES

Arlt R., Rendtel J., 1994, WGN, 22, 167
Bel'kovich O. I., Sulejmanov N. I., Tokhtas'ev V. S., 1984, Bull. Astron. Inst. Czech., 35, 123
Brown P., Jones J., 1995, Earth, Moon, Planets, 68, 223
Brown P., Rendtel J., 1996, Icarus, 124, 414
Browne I. B., Bullough K., Evans S., Kaiser T. R., 1956, Proc. Phys. Soc., B69, 83
Bullough K., 1954, Jodrell Bank Ann., 1, 68
Elford W. G., Hawkins G. S., 1964, Harvard Radio Meteor Project Research Report No. 9, SAO
Elford W. G., Cervera M. A., Steel D. I., 1994, MNRAS, 270, 401
Flemming D. E. B., Hawkes R. L., Jones J., 1993, in Stoh J., Williams I. P., eds, Meteoroids and their Parent Bodies. Astron. Inst. Slovak Acad. Sci., Bratislava, p. 261
Froschle C., Scholl H., 1982, A&A, 111, 346
Greenhow J. S., Hall J. E., 1960, MNRAS, 121, 183
Gustafson B. A. S., 1989, A&A, 225, 553
Hajduk A., McIntosh B. A., Šimek M., 1974, BAC, 25, 305
Hocking W. K., 1997, J. Geophys. Res. D, 102, 687

Hocking W. K., Thayaparan T., 1997, JGRD, 102, 833
Hughes D. W., Taylor I. W., 1977, MNRAS, 181, 517
Hughes D. W., Williams I. P., Fox K., 1981, MNRAS, 195, 625
Jones J., 1977, BAC, 28, 272
Jones J., 1978, MNRAS, 183, 539
Jones J., Morton J. D., 1982, MNRAS, 200, 281
Jones J., Jones W., 1993, MNRAS, 261, 605
Jones J., Webster A. R., 1992, in Harris A. W., Bowell E., eds, Asteroids, Comets, Meteors 1991. LPI Press, Houston, p. 273
Kaiser T. R., 1955, J. Atmos. Terr. Phys., 2, 119
Kaiser T. R., 1960, MNRAS, 121, 284
Kaiser T. R., Closs R. L., 1952, Phil. Mag., 43, 1
Luu J. X., 1993, Icarus, 104, 138
McIntosh B. A., 1966, Can. J. Phys., 44, 2729
McIntosh B. A., Šimek M., 1980, BAC, 31, 39
McIntosh B. A., Šimek M., 1984, BAC, 35, 14
McKinley D. W. R., 1961, Meteor Science and Engineering. McGraw-Hill, New York
Murray C. D., Hughes D. W., Williams I. P., 1980, MNRAS, 180, 733
Ohtsuka K., Toshikawa M., Watanabe J.-I., 1995, PASJ, 47, 477
Plavcova Z., 1962, BAC, 13, 176
Poole L. M. G., Kaiser T. R., 1967, Planet. Space Sci., 15, 1131
Poole L. M. G., Hughes D. W., Kaiser T. R., 1972, MNRAS, 156
Rendtel J., Arlt R., McBeath A., 1995, Handbook for Visual Meteor Observers. IMO, Potsdam
Rendtel J., Brown P., Molau S., 1996, MNRAS, 279, L31
Šimek M., 1985, BAC, 36, 270
Šimek M., 1987, 10th European Regional Astronomical Meeting, in Ceplecha Z., Pecina P., eds, Astron. Inst. Czech. Acad. Sci., Prague, p. 199
Šimek M., McIntosh B. A., 1991, BAC, 42, 124
Thayaparan T., 1995, PhD thesis, University of Western Ontario
Watanabe J.-I., Nakamura T., Tsutsumi M., Tsuda T., 1992, PASJ, 44, 677
Williams L. P., Wu Z., 1993, MNRAS, 264, 659